An element by element spectral element method for elastic wave modeling*

LIN Weijun[1**], WANG Xiuming[1,2] and ZHANG Hailan[1]

(1. Institute of Acoustics, Chinese Academy of Sciences, Beijing 100080, China; 2. CSIRO petroleum, ARRC, PO BOX 1130, Technology Park, Bentley, WA 6102, Australia)

Received March 25, 2005; revised April 18, 2005

Abstract The spectral element method which combines the advantages of spectral method with those of finite element method, provides an efficient tool in simulating elastic wave equation in complex medium. Based on weak form of elastodynamic equations, mathematical formulations for Legendre spectral element method are presented. The wave field on an element is discretized using high-order Lagrange interpolation, and integration over the element is accomplished based upon the Gauss-Lobatto-Legendre integration rule. This results in a diagonal mass matrix which leads to a greatly simplified algorithm. In addition, the element by element technique is introduced in our method to reduce the memory sizes and improve the computation efficiency. Finally, some numerical examples are presented to demonstrate the spectral accuracy and the efficiency. Because of combinations of the finite element scheme and spectral algorithms, this method can be used for complex models, including free surface boundaries and strong heterogeneity.

Keywords: **spectral element, Legendre polynomial, elastic wave modeling, element by element.**

Despite the ever-growing power of modern computers, the modeling of large-scale elastic wave propagation is still a challenging problem now. Considerable efforts have been devoted to developing highly accurate numerical techniques for the solution of elastic wave equations.

Finite difference method (FDM), finite element method (FEM), and spectral method are three options usually used in elastic wave modeling.

The FDM can be seen as a point collocation method (The residual is forced to be zero in the set of collocation points), but it does not use an approximate solution. A discrete differential operator around the collocation points can be derived using truncated Taylor-series. The error of finite difference approximation is determined by both the number of collocation points chosen and the truncation error in the Taylor series used to approximate the differential operator[1]. Since it is easy and efficient, FDM has been widely used in computational seismology, exploration geophysics and so on. Similar to a lower-order FEM, lower order FDM requires a large number of cells to achieve an expected accuracy[2,3], while high-order staggered FDM cannot handle a free surface and complex configuration efficiently[4].

The well known FEM is a kind of Galerkin weighted-residual method[5], in which the domain of the basis function and test function chosen are the same, and the global computational domain is divided into small elements. The basis function is defined in each element, and an approximate result is obtained by minimizing the residual in a global domain[6]. FEM allows a natural treatment of free-boundary conditions, and it is suitable for heterogeneous elastic media with complex geometries[7,8]. However, these methods are computationally expensive compared to the explicit FDM[9]. This may be the main reason why this method has attracted a little attention from geophysicists. Also, low-order FEM exhibits poor dispersion properties[10], while conventional high-order FEM unfortunately generates spurious waves[11].

Spectral methods, with their basis functions being infinite differentiable functions on their global domain, are able to achieve an expected accuracy using few grid points per wavelength[12]. In order to deal with more general boundary conditions, the set of truncated Fourier series is usually replaced by a set of orthogonal polynomials such as Chebyshev or Legendre polynomials in a space domain[13]. A limitation of the approach is that the non-uniform spacing of the

* Supported by National Natural Science Foundation of China (Grant No. 10134020), the Fellowship of Chinese Academy of Sciences in China, and the fellowship of the Abdus Salam International Centre for Theoretical Physics of UNESCO in Italy.

** To whom correspondence should be addressed. E-mail: linwj@mail.ioa.ac.cn

orthogonal polynomial collocation points put stringent constraints on the time-step[14]. Like the FDM, the spectral method cannot handle complex geometries and curved free surface easily. The method of curvilinear co-ordinate system[14] and domain decomposition method[15] were implemented to overcome this drawback, but this also brings expensive computation.

A spectral element method (SPEM), originally proposed by Patera for fluid dynamics[16], combines the finite-element scheme with the spectral expansion on each element, to greatly improve the computation accuracy. Compared with FEM, the requirement of computational time and memory can be reduced by using sparse grid in SPEM. Seriani was the first one to introduce the SPEM for forward elastic wave propagation problems, and the related work has been extended greatly in recent years[11,17—20]. However, some special techniques or parallel computation are still needed to deal with some large scale problems[18,21].

The basic idea of the SPEM is that it uses a spectral expansion on each element. At the same time, it chooses a special shape function defined as truncated orthogonal polynomials. It is similar to the sine and cosine terms in a Fourier series, which leads to a high rate of convergence of a series to represent the solution. The procedure of the method is as follows: (1) decompose the computational domain into many sub-domains; (2) express the desired solution as a truncated expansion of a product of orthogonal polynomials that can be Chebyshev or Legendre polynomials in each sub-domain; (3) compute the solution by solving the weak formulation of the orthogonal problem via the Galerkin approach.

As mentioned above, there are two kinds of orthogonal polynomials used in the SPEM: Chebyshev polynomials[17,18,20] and Legendre polynomials[11,21]. Both of them are the eigenfunctions of the singular Sturm-Liouville equation. However, their different properties lead to different approaches in the SPEM.

This paper is based on the Legendre polynomials, which leads to a diagonal mass matrix and a simple algorithm. In addition, in order to reduce the large memory and computation cost required in the method, an element by element approach[6,18] is first introduced in our Legendre SPEM, and its effect in reducing the memory and computation cost has been analyzed in detail. Moreover, some numerical examples are computed to demonstrate the spectral accuracy and the efficiency obtained by the Legendre SPEM based upon element by element approach in dealing with complex problem.

1 Mathematical formulation

1.1 Elastic wave equation and its weak form

When we consider an elastic inhomogeneous medium occupying an open, bounded region $\Omega \subset R^{n_d}$, where n_d is the number of space dimension, the strong form of the elastic wave equation can be formally stated as

$$\rho \boldsymbol{u}_{i,tt} = \boldsymbol{\sigma}_{ij,j} + \boldsymbol{f}_i, \quad \text{in} \quad \Omega \times [0, T], \tag{1}$$

$$\boldsymbol{u}_i = \boldsymbol{g}_i, \quad \text{in} \quad \Gamma_{gi} \times [0, T], \tag{2}$$

$$\boldsymbol{\sigma}_{ij} n_j = \boldsymbol{h}_i, \quad \text{in} \quad \Gamma_{hi} \times [0, T], \tag{3}$$

where $\boldsymbol{u}_i$ is the displacement component in the x_i-direction; x_i is a coordinate axis with $i = 1, \cdots, n_d$; $\boldsymbol{\sigma}_{ij}$ is the stress tensor, which is defined by the generalized Hook's law: $\boldsymbol{\sigma}_{ij} = \boldsymbol{c}_{ijkl}\boldsymbol{u}_{k,l}$ ($\boldsymbol{c}_{ijkl}$ is the elastic tensor); $t \in [0, T]$ is the time of interest; Γ_{gi} and Γ_{hi} are the displacement boundary and stress boundary, respectively; $\boldsymbol{g}_i$ and $\boldsymbol{h}_i$ are called the prescribed boundary displacements and tractions, respectively.

By using the method of weighted residuals, the weak form of the elastic wave equation can be written as

$$(\boldsymbol{w}, \rho \ddot{\boldsymbol{u}}) + a(\boldsymbol{w}, \boldsymbol{u}) = (\boldsymbol{w}, \boldsymbol{f}) + (\boldsymbol{w}, \boldsymbol{h})_\Gamma, \tag{4}$$

where $\boldsymbol{u}(t) \in \delta_t$ is a trial solution, and $w \in \upsilon$ is a test function. δ_t denotes a trial solution domain. For any given, $\boldsymbol{u}(t) \in \delta_t$, $\boldsymbol{u}(t)$ satisfies $\boldsymbol{u}_i = \boldsymbol{g}_i$ in displacement boundary and has the square-integrable generalized first derivative in the domain. Whereas υ denotes a test function space, and its member satisfies $w_i = 0$ on Γ_{gi} and also has a square-integrable generalized first derivative in the defined domain. The inner product in Eq. (4) can be stated as

$$(\boldsymbol{w}, \rho \ddot{\boldsymbol{u}}) = \frac{\mathrm{d}^2}{\mathrm{d}t^2}(\boldsymbol{w}, \rho \boldsymbol{u}) = \frac{\mathrm{d}^2}{\mathrm{d}t^2}\int_\Omega \rho \boldsymbol{w}_i \boldsymbol{u}_i \mathrm{d}\Omega, \tag{1}$$

$$a(\boldsymbol{w}, \boldsymbol{u}) = \int_\Omega \boldsymbol{w}_{(i,j)} \boldsymbol{c}_{ijkl} \boldsymbol{u}_{(k,l)} \mathrm{d}\Omega, \tag{6}$$

$$(\boldsymbol{w}, \boldsymbol{f}) = \int_\Omega \boldsymbol{w}_i \boldsymbol{f}_i \mathrm{d}\Omega, \tag{7}$$

$$(\boldsymbol{w}, \boldsymbol{h})_\Gamma = \sum_{i=1}^{n_{sd}} \left(\int_{\Gamma_{hi}} \boldsymbol{w}_i \boldsymbol{h}_i \mathrm{d}\Gamma \right), \tag{8}$$

where $\boldsymbol{w}_{(i,j)} = \dfrac{\boldsymbol{w}_{i,j} + \boldsymbol{w}_{j,i}}{2}$, and $\boldsymbol{w}_{k,l} = \partial \boldsymbol{w}_k / \partial x_l$, for $k, l = 1, \cdots, n_d$.

1.2 Spatial discretization

Similar to the FEM, the original physical domain Ω is discretized into n_e non-overlapping elementary quadrilaterals Ω_e. This partition $\Omega = \bigcup \Omega_e$ of the domain is generically referred to as the quadrangulation and is denoted as L^h, where h is the mesh parameter, a scalar characterizing the refinement of the spectral element mesh. And the restriction of the test-function w to the element Ω_e is denoted $w^h|_{\Omega_e}$. Let us denote $\Lambda = [-1, 1]$ and the reference volume Λ^{n_d}, which is a square or a cube depending on the spatial dimension n_d of the problem. For each element $\Omega_e \in L^h$, suppose that there exists an invertible mapping function F_e between the reference volume and a local coordinate system of the element Ω_e, defined as $F_e: \Lambda^{n_d} \rightarrow \Omega_e$, we can then use this mapping between the physical domain and the reference domain, and vice versa. Associating with the spatial discretization L^h, we denote δ_t^h the trial solution space defined in element, and υ^h the test function space defined in element. Choosing the same function space for δ_t^h and υ^h, the Galerkin statement of the discrete weak form can be obtained:

$$(\boldsymbol{w}^h, \rho \ddot{\boldsymbol{u}}^h) + a(\boldsymbol{w}^h, \boldsymbol{u}^h) = (\boldsymbol{w}^h, \boldsymbol{f}) + (\boldsymbol{w}^h, \boldsymbol{h})_\Gamma, \tag{9}$$

where $\boldsymbol{u}^h(t) \in \delta_t^h$, $\boldsymbol{w}^h \in \boldsymbol{\upsilon}^h$.

After spatial discretization, additional grids (basis points or interpolation points) can be introduced in each element domain to increase the accuracy of the approximated result, which is called high order method in FEM. However, in the way of choosing the additional grid points and shape functions to approximate the trial solution, SPEM shows that it is different from a general high order FEM. For convenience, at the moment we only consider the two-dimensional problem.

Figure 1 shows the Legendre discretization of the reference element for $N = 4$, which means the order of orthogonal polynomials we used in one dimension is 4. In Legendre SPEM, in order to take advantage of efficient sum-factorization techniques, and to improve the conditioning and sparsity of the resulting set of algebraic equations, the additional grids (basis points or interpolation points) are located at the tensor product of the Legendre Gauss-Lobatto points (collocation points) in each dimension, and a special shape function defined with truncated orthogonal polynomials is chosen, which leads to a high rate of convergence.

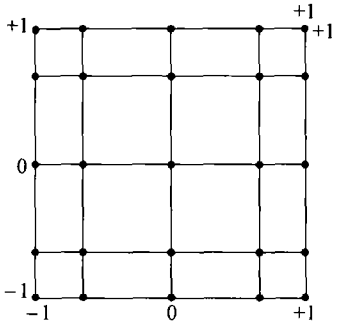

Fig. 1. Legendre discretization of the reference element for $N = 4$.

On each element, the solution is approximated by the Lagrange interpolation of the shape functions defined at collocation points. That is, a function $\boldsymbol{u}(\xi, \eta)$, defined on the reference square Λ^{n_d}, can be approximated as

$$\begin{aligned}\tilde{\boldsymbol{u}}(\xi, \eta) &= \sum_{i=0}^{N}\sum_{j=0}^{N} \tilde{\boldsymbol{u}}_{ij}\varphi_i(\xi)\varphi_j(\eta) \\ &= \sum_{i=0}^{N}\sum_{j=0}^{N} \tilde{\boldsymbol{u}}_{ij}\phi_{ij}(\xi, \eta),\end{aligned} \tag{10}$$

where $\tilde{\boldsymbol{u}}_{ij} = \boldsymbol{u}(\xi^i, \eta^j)$ are the values of $\boldsymbol{u}$ at the grid points, the shape function $\phi_{ij}(\xi, \eta)$ is the tensor product of the basis function $\varphi_i(\zeta)$ defined in one dimension, that is $\phi_{ij}(\xi, \eta) = \varphi_i(\xi)\varphi_j(\eta)$. $\varphi_i(\zeta)$ can be expanded in a truncated orthogonal polynomials and satisfying the relation $\varphi_i(\zeta_k) = \delta_{ik}$ within the Λ, and identically zero outside. Here, δ_{ik} denotes the Kronecker delta symbol and ζ stands for ξ or η. Details of the Legendre polynomials are given in the Appendix.

Since it is difficult to compute the inner product in Eq. (9) analytically by using Legendre polynomials, the discrete inner product should be defined to approximate the inner product in Eqs. (5)—(8). Also, the discrete inner products are based on the tensor-product of 1-D Gauss-Lobatto-Legendre formulas. The quadrature points are the same as the basis points so the calculation is easy to be performed, and for $N+1$ quadrature points, all polynomials of degree $\leqslant 2N-1$ can be integrated exactly[22]. In this case, the discrete inner products in Eq. (9) are defined as[11]:

$$\begin{aligned}(\boldsymbol{w}_N^h, \rho \boldsymbol{u}_N^h)_N = &\sum_{e=1}^{n_e}\sum_{i,j=0}^{N} \boldsymbol{w}_N^h|_{\Omega_e}(\xi^i, \eta^j) \\ &\cdot \boldsymbol{u}_N^h|_{\Omega_e}(\xi^i, \eta^j) \cdot \rho \cdot |\boldsymbol{J}_e(\xi^i, \eta^j)| \cdot \boldsymbol{\omega}_{ij},\end{aligned} \tag{11}$$

$$a_N(\boldsymbol{w}_N^h, \boldsymbol{u}_N^h)_N = \sum_{e=1}^{n_e} \sum_{i,j=0}^{N} \tilde{\nabla} \boldsymbol{w}_N^h \mid_{\Omega_e}(\xi^i, \eta^j) : \boldsymbol{c}(\xi^i, \eta^j) : \tilde{\nabla} \boldsymbol{u}_N^h \mid_{\Omega_e}(\xi^i, \eta^j) \cdot \mid \boldsymbol{J}_e(\xi^i, \eta^j) \mid \boldsymbol{\omega}_{ij}, \quad (12)$$

where $\boldsymbol{J}_e$ is the Jacobian matrix of the co-ordinate transformation at an element level, weight $\boldsymbol{\omega}_{ij} = \boldsymbol{\omega}_i \boldsymbol{\omega}_j$, and $\tilde{\nabla}$ is the pull back of the gradient operator on the reference volume Λ^{n_d}:

$$\nabla_X \boldsymbol{w}_N^h \mid_{\Omega_e} = \tilde{\nabla} \boldsymbol{w}_N^h \mid_{\Omega_e}(\zeta) = \nabla_\zeta \boldsymbol{w}_N^h \mid_{\Omega_e}(\zeta) \cdot \left(\frac{\partial \zeta}{\partial (F_e(\zeta))} \right). \quad (13)$$

Like FEM approach, we get a set of second order ordinary differential equations with respect to time for wave field displacements expressed by

$$\boldsymbol{M}\ddot{\boldsymbol{U}}(t) + \boldsymbol{K}\boldsymbol{U}(t) = \boldsymbol{F}(t), \quad (14)$$

with $\boldsymbol{U}(0) = \{\boldsymbol{U}_0\}$, $\dot{\boldsymbol{U}}(0) = \{\dot{\boldsymbol{U}}_0\}$ as the initial conditions for the initial displacement and initial particle velocity, where the unknown vector $\boldsymbol{U}$ contains the values of the discrete solution $\tilde{\boldsymbol{u}}$ at all Legendre collocation points in all elements, $\boldsymbol{M}$ is the global mass matrix, $\boldsymbol{K}$ is the global stiffness matrix, and $\boldsymbol{F}$ is the force vector. They can be computed using the matrix element summation over all the element matrixes of $\boldsymbol{M}^{(e)}$ and $\boldsymbol{K}^{(e)}$. The contributions from nodes which are common to an element pair are summed to enforce the continuity requirement of the solution on the element boundaries. With the help of the mapping from a physical element to reference element, all the element matrixes can be computed in a reference volume.

An attractive property of the Legendre approach is that, in contrast with classical FEM, due to the consistent integration scheme and the use of Legendre-Gauss-Lobatto formulas, the global mass matrix $\boldsymbol{M}$ is always diagonal, which leads to a fully explicit scheme and makes the algorithm easy to implement.

1.3 Time discretization

In order to solve the system of linear equation (14), we must integrate over the time interval $[0, T]$. This may be done in a direct way by discretizing the time variable as $t_n = n\Delta t$, $0 \leqslant n \leqslant N_T$, where $\Delta t = T/N_T$, and N_T is the total number of time steps.

In our Legendre approach, since the mass matrix $\boldsymbol{M}$ is diagonal, we can implement the time integration of Eq. (14) numerically by a central difference method, which is conditionally stable. However, when $\boldsymbol{M}$ is diagonal, it is explicit. When the choice of the time step is not restricted too much, as is often true in elastic wave propagation problems, the central difference method is generally one of the most economical procedures and is thus widely used[6]. The solution at time $(n+1)\Delta t$ is obtained by solving the following system of linear equations directly:

$$\left(\frac{1}{\Delta t^2} \boldsymbol{M} \right) \boldsymbol{U}^{n+1} = \boldsymbol{F}^n - \left(\boldsymbol{K} - \frac{2}{\Delta t^2} \boldsymbol{M} \right) \boldsymbol{U}^n - \left(\frac{1}{\Delta t^2} \boldsymbol{M} \right) \boldsymbol{U}^{n-1}. \quad (15)$$

1.4 Element by element technique

The idea of an element by element algorithm firstly appeared in FEM[6]. Seriani introduced this idea into the Chebysheve Polynomial SPEM in 1997[18]. Also, this algorithm can be employed for the Legendre Polynomial SPEM, which is the major part in our work.

Generally, global mass matrix and stiffness matrix should be formed to solve an elastic wave problem whether SPEM or FEM is used, which requires a large memory space even if one-dimensional variable band storage strategy is used. This is true especially in SPEM, where the memory space increases rapidly as the order of polynomials increases. In the time integration procedure, the most computational intensive part is a matrix-vector production (see Eq. 15), such as $\boldsymbol{S} \cdot \boldsymbol{p}_k$, where $\boldsymbol{S}$ is a global matrix, and $\boldsymbol{p}_k$ is a global vector. Considering the sparse character of these global matrixes, most of the computation in $\boldsymbol{S} \cdot \boldsymbol{p}_k$ is useless. From element point of view, the result vector of $\boldsymbol{S} \cdot \boldsymbol{p}_k$ can be computed at the level of individual elements. This can be written as

$$\boldsymbol{S} \cdot \boldsymbol{p}_k = \left(\sum_e \tilde{\boldsymbol{S}}^e \right) \boldsymbol{p}_k = \sum_e (\tilde{\boldsymbol{S}}^e \cdot \tilde{\boldsymbol{p}}_k^e) = \sum_e \tilde{\boldsymbol{v}}_k^e = \boldsymbol{v}_k, \quad (16)$$

where $\tilde{\boldsymbol{S}}^e$ and $\tilde{\boldsymbol{p}}_k^e$ are the element contributions to the global matrix $\boldsymbol{S}$ and global vector $\boldsymbol{p}_k$, respectively. In the above equation, instead of computing the multiplication of global matrix with the global vector, it is calculated in the local element sense. The detailed treatment is that, first, element matrix is calculated, and the element vector is formed using the global and local links, i.e. the vector $\tilde{\boldsymbol{p}}_k^e$ is scattered from the global vector $\boldsymbol{p}_k$ with the help of their relationship be-

tween $\tilde{\boldsymbol{p}}_k^e$ and $\boldsymbol{p}_k$. Then their products are carried out locally using matrix-vector multiplication algorithms, and the element vector $\tilde{\boldsymbol{v}}_k^e = \tilde{\boldsymbol{S}}^e \cdot \tilde{\boldsymbol{p}}_k^e$ is obtained. After that, $\tilde{\boldsymbol{v}}_k^e$ is collected to the global vector $\boldsymbol{v}_k$. With the help of scattering and collecting between the global matrix and element matrix through the mapping, the global matrix $\boldsymbol{S}$ is not really used, and only the element matrix $\tilde{\boldsymbol{S}}^e$ is stored in our method, which drastically reduces the memory requirement and computation cost.

A square computation area Ω with $m \times m$ non-overlapping quadrilateral elements is used here as an example. The order of the Legendre polynomials is n, and the total number of points of the global grid is $(mn+1)\times(mn+1)$. Then, the size of the global matrix $\boldsymbol{S}$ will be $S_g = [2\times(mn+1)\times(mn+1)]^2$. If we use the element by element method, the size of the element matrix $\tilde{\boldsymbol{S}}^e$ will be $[2\times(n+1)\times(n+1)]^2$, since there are $m \times m$ elements, the total size is required to be $S_e = m\times m\times[2\times(n+1)\times(n+1)]^2$. Therefore,

$$\frac{S_g}{S_e} \approx m^2 \times \left(\frac{n}{n+1}\right)^4. \tag{17}$$

Assume $m = 100$ and $n = 6$, $\frac{S_g}{S_e} \approx 5400$. That is, the memory required will reduce less than 5000 times if the element by element technique is used.

Now, let us consider the computation cost. In a global matrix-vector production $\boldsymbol{S}\cdot\boldsymbol{p}_k$, the total number of multiplications $T_g = [2\times(mn+1)\times(mn+1)]^2$. However, in the element by element technique, the global matrix-vector production is transformed into $m \times m$ times element matrix-vector production, and its total number of multiplications $T_e = m\times m\times[2\times(n+1)\times(n+1)]^2$. Then, we can obtain

$$\frac{T_g}{T_e} \approx m^2 \times \left(\frac{n}{n+1}\right)^4. \tag{18}$$

That is, through the element by element technique, the computation cost can be reduced drastically in the same amount as that of reduced memory space required.

Moreover, since most of the work in Legendre SPEM can be completed in local element if the element by element approach is used, this Legendre SPEM is suitable for being paralleled naturally, and a high degree of vectorization and parallelization can be obtained.

2 Numerical examples

To demonstrate the accuracy and efficiency of the spectral element method, we simulate some specific problems and compare the result of Legendre SPEM with the corresponding analytical solution or solution of the other method. All of these examples are completed in personal computer by using the element by element approach.

2.1 A homogeneous medium

First, we compare the analytical and numerical solutions for an impulsive force acting in an elastic homogeneous medium. The test model is shown in Fig. 2, which consists of a square domain with the side length of $L = 2560$ m, and the compressional and shear velocities, and density, given by $v_p = 2900$ m/s, $v_s = 1611$ m/s, $\rho = 1900$ kg/m^3, respectively. A horizontal band-limited force is applied at the point $S(-300\text{ m}, -300\text{ m})$. The wavelet function is the first derivative of a Gaussian function, and its central frequency is 10 Hz. The record point R is located at (300 m, 300 m).

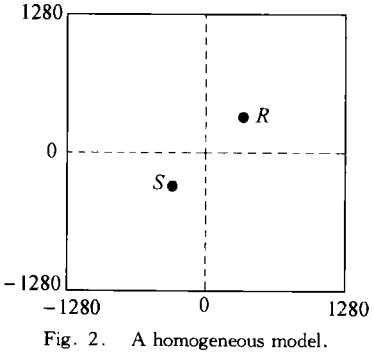

Fig. 2. A homogeneous model.

In our SPEM, the model is discretized using 64 by 64 square spectral elements, the size of each element is 40 m by 40 m. We use a polynomial degree $N = 4$ in each element. The time step Δt is 0.8 ms. An absorbing strip is added outside the boundary to simulate the open radiation conditions, which uses a damping mechanism to attenuate the elastic energy smoothly.

Fig. 3 displays a snapshot of horizontal velocity V_x at time 0.36 s, which is the result of SPEM, where the P- and S-waves can be easily recognized. Fig. 4(a) and Fig. 4(b) are the comparisons between analytical and numerical solutions for horizontal velocity and vertical velocity waveforms recorded at point R, respectively. In each figure, the real line denotes

the result of analytical method, while the dash line denotes the result of SPEM. The dot line denotes the difference between the waveforms by the two methods, which has been amplified by a factor 3 for easy visualizations. The agreement is excellent with a maximum error of nearly 2% for all waveforms that we record.

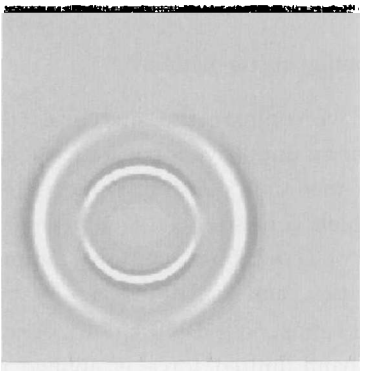

Fig. 3. A snapshot of V_x at 0.36 s.

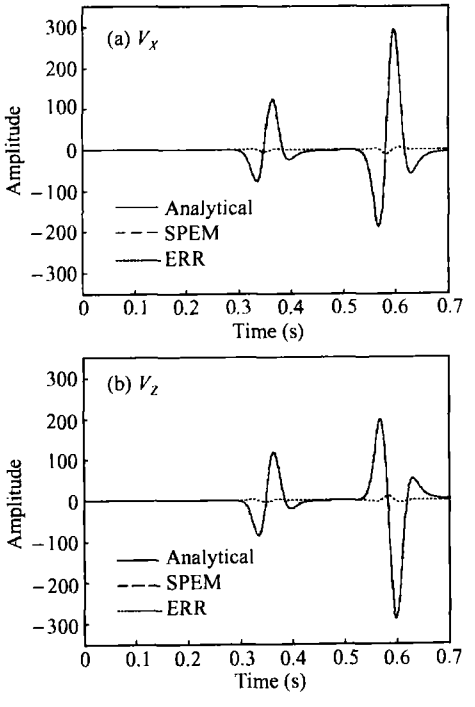

Fig. 4. Comparisons between the analytical and numerical solutions in response to a horizontal force in an elastic homogeneous medium for (a) the horizontal velocity, and (b) the vertical velocity, respectively.

2.2 A homogeneous medium with a horizontal layer

In this section, we consider a piecewise homogeneous medium with a horizontal layer. The test model is shown in Fig. 5, which is also a square domain with a side length of $L = 2560$ m, but it consists of two quadrilateral formations which constitute a horizontal layer centered at the square domain. The down formation is a slow formation, with its compressional and shear velocities, and density, given by $v_{p1} = 2900$ m/s, $v_{s1} = 1611$ m/s, and $\rho_1 = 1900$ kg/m^3, respectively. The upper formation is a fast one, with its compressional and shear velocities, and its density, given by $v_{p2} = 3600$ m/s, $v_{s2} = 2057$ m/s, and $\rho_2 = 2680$ kg/m^3, respectively. The same horizontal band-limited force used in Section 2.1 is applied at point S which lies at point (0 m, −225 m) in the lower formation. Now, we use two record points lying in the lower and upper formations, respectively. The first record point R_1 is at (500 m, −275 m), while the second one R_2 is at (500 m, 275 m).

A pseudo spectral (PS) method is used to compare with the SPEM. For computing spatial derivatives, Fourier differential operators are used in both horizontal and vertical directions in the PS method. According to the model in Fig. 5, these operators would have infinite accuracy (within a machine precision) up to two points per minimum wavelength (the Nyquist wave number).

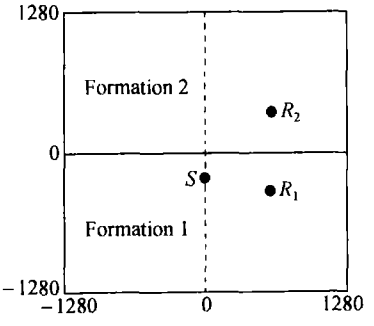

Fig. 5. The model of homogeneous medium with a horizontal layer.

The PS domain is composed of 256×256 square elements, and each element has a size of 10 m in the horizontal and vertical directions. The time step is $\Delta t = 0.8$ ms. In order to avoid wraparound caused by the periodic properties of the Fourier method, absorbing regions are placed along the boundaries in the horizontal and vertical directions.

In the SPEM, the model is discretized using 64×64 square spectral elements, and we use a polynomial degree $N = 4$ in each element. Considering the location of the layer is defined differently between SPEM and PS methods, the size of each element in the SPEM is determined as 50 m × 50 m. Therefore,

the SPEM computation domain is larger than that of the PS method. However, it will not affect the results of interest. The time step in the SPEM is $\Delta t = 0.8$ ms.

Fig. 6 shows the snapshot of horizontal velocity V_x simulated by the SPEM at the time of 0.36 s, where the direct P- and S-waves reflect P-and S-waves, refracted P-and S-waves, also including head waves, can be recognized easily. Fig.7(a) and Fig.7(b) are the comparisons of the recorded horizontal velocity and vertical velocity waveforms at point R_1 for the PS and SPEM, respectively. Fig.8(a) and Fig.8(b) compare the recorded horizontal velocity and vertical velocity waveforms at point R_2 of PS and SPEM, respectively. In each figure, the real line denotes the result of PS, and the dash line denotes the result of SPEM. Both of them show an excellent agreement between these two methods, which shows SPEM acquires the spectral accuracy using much lower order of orthogonal polynomials in this piecewise homogeneous medium.

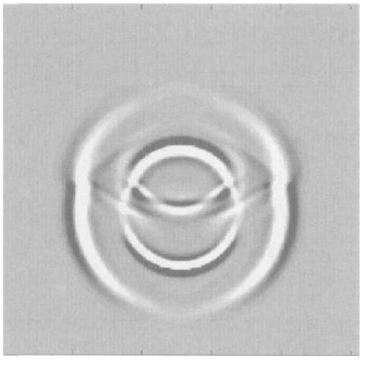

Fig. 6. Snapshot of V_x at 0.36 s.

2.3 A homogeneous medium with an inclined layer

Then, we consider a piecewise homogeneous medium with an inclined layer. The test model is shown in Fig. 9, which is also a square domain with the side length of $L = 2560$ m. This model consists of two quadrilateral formations which constitute an inclined layer. The inclined layer crosses the center of the square domain and forms an inclined angle of 18.43° with the horizontal axis. The lower formation is a slow formation, the upper formation is a fast one, and their compressional and shear velocities, and density are the same as those of Section 2.2. The same horizontal band-limited force source used in Section 2.1 is applied at point S (0 m, −300 m) which lies in the lower formation.

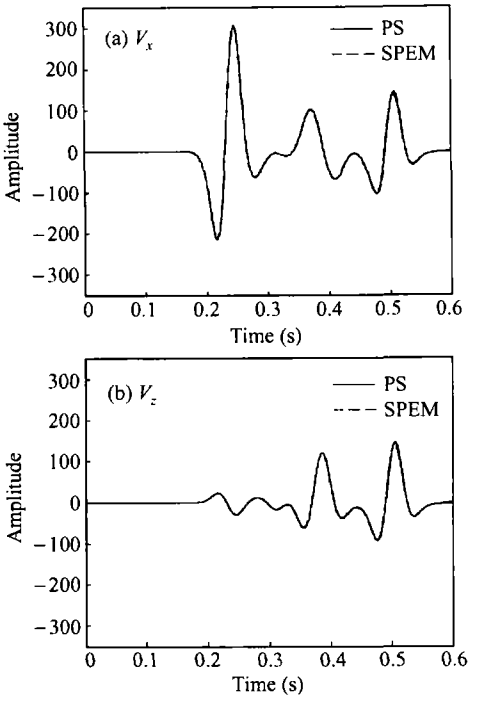

Fig. 7. Waveform comparisons received at R_1, excited by a horizontal force in an elastic homogeneous medium, with a horizontal layer for (a) the horizontal velocity component, and (b) the vertical velocity component, respectively.

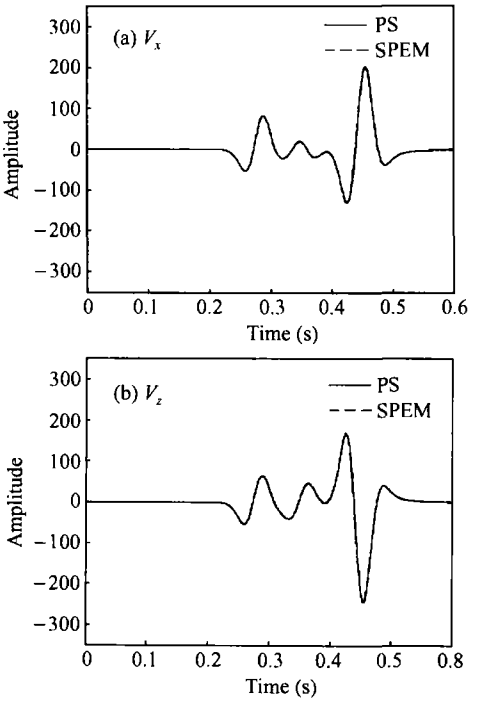

Fig. 8. Waveform comparisons received at R_2, excited by a horizontal force source in an elastic homogeneous medium with a horizontal layer for (a) the horizontal velocity component, and (b) the vertical velocity component, respectively.

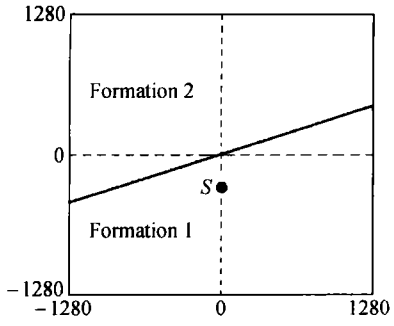

Fig. 9. A model of a homogeneous medium with an inclined layer.

Due to the inclined layer, only the SPEM is used for this model. It is discretized using 64 by 64 quadrilateral spectral elements instead of the square elements, and an order of the polynomials $N = 4$ in each of the element. The time step is $\Delta t = 0.5$ ms. In this calculation free boundary conditions on each side are used.

Fig.10(a), (b), (c), and (d) show the snapshots of horizontal velocity component V_x by SPEM at time 0.15 s, 0.25 s, 0.35 s, and 0.45 s, respectively. The propagation of the elastic waves in this model with an inclined layer is shown clearly, which demonstrates the ability of the SPEM to deal with complex situations in elastodynamics.

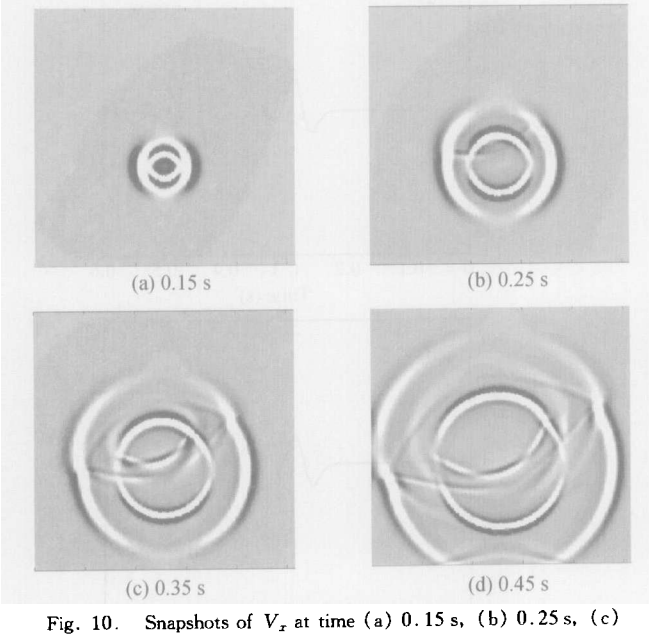

Fig. 10. Snapshots of V_x at time (a) 0.15 s, (b) 0.25 s, (c) 0.35 s, and (d) 0.45 s.

2.4 A homogeneous medium with a curved free surface

Now, we describe the application of this Legendre SPEM to study a two-dimensional smooth topographical profile. The mesh for this model is shown in Fig. 11. The topography is described by a Gaussian function (the maximum height is 160 m). The material properties of the medium are $c_p = 3200$ m/s, $c_s = 1847.5$ m/s, and $\rho = 2200$ kg/m^3. The size of the model is 4000 m × 1600 m, and the height of the hill is 160 m. The mesh is composed of 50 × 20 elements, with a polynomial order of $N = 6$ used in each direction, leading to a total number of collocation points of 36421. On all the boundaries of the grid except the upper free surface, an absorbing condition is imposed. The same horizontal band-limited force used in Section 2.1 is applied at point S(1360 m, 1440 m), with the central frequency of 7 Hz, and the time step of $\Delta t = 0.5$ ms.

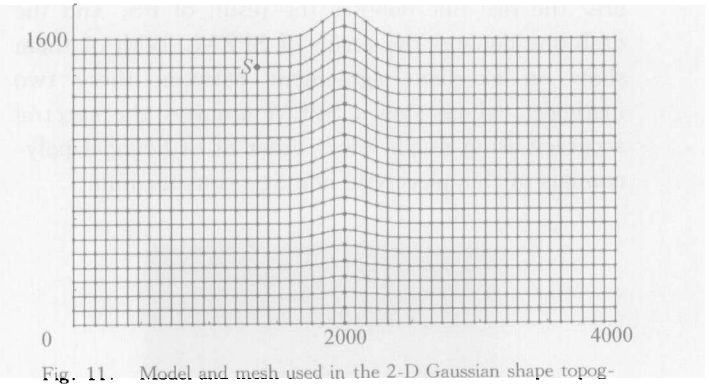

Fig. 11. Model and mesh used in the 2-D Gaussian shape topography.

Fig. 12 illustrates four snapshots of horizontal velocity V_x at time 0.1 s, 0.2 s, 0.3 s, and 0.4 s, respectively. The propagation of the elastic waves in this model is shown clearly, which demonstrates the ability of the SPEM to simulate the complex media with a curved free surface.

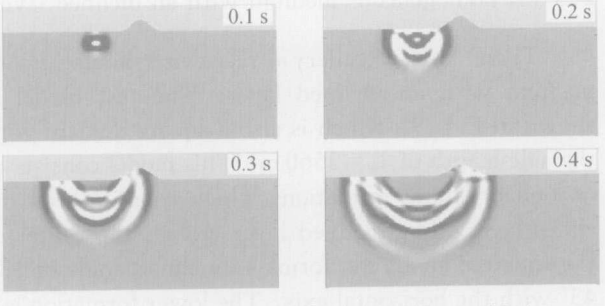

Fig. 12. Snapshot of V_x at 0.1 s, 0.2 s, 0.3 s, and 0.4 s, respectively.

3 Discussion and conclusion

A high-order element by element Legendre SPEM is proposed. This method, combining the ad-

vantages of a spectral method with those of a FEM in each element, provides an efficient tool in simulating elastic wave equation in complex medium.

The mathematical formulations for the Legendre SPEM are presented based on the weak form of elastodynamic equation. Due to the consistent integration scheme and the use of Legendre-Gauss-Lobatto formulas, a diagonal global mass matrix is obtained, which can lead to a fully explicit scheme and reduce the computation time. In addition, an element by element technique is first introduced in Legendre SPEM which can reduce the memory and computation cost drastically. The numerical examples show some capabilities of the accuracy and flexibility of the Legendre SPEM based upon the element by element technique. The numerical results of the SPEM are in good agreement with the analytical solutions for a simple model, which validates our algorithm. Because of the flexibility of the FEM and the spectral precision, this method can be effectively used in traction free surface and complicated media for simulating elastic wave propagation.

Acknowledgement The authors would like to thank Dr. Geza Seriani, Instituto Nazonnale di Oceangrafia e di Geofisica Sperimentale, Italy, for his help and suggestions.

Appendix

The Legendre polynomials $\{L_k(x), k=0,1,\cdots\}$ are the eignfunctions of the singular Sturm-Liouville equation[22]:

$$((1-x^2)L_k'(x))' + k(k+1)L_k(x) = 0. \tag{A1}$$

The Legendre polynomials are othorgonal with the weight $w(x)=1$. If $L_k(x)$ is normalized so that $L_k(1)=1$, then for any k,

$$L_k(x) = \frac{1}{2^k}\sum_{l=0}^{[k/2]}(-1)^l\binom{k}{l}\binom{2k-2l}{k}x^{k-2l}, \tag{A2}$$

where $[k/2]$ denotes the integral part of $k/2$. And the Legendre-Gauss-Lobatto points and weights are defined as

$$x_0 = -1, \quad x_N = 1,$$
$$x_j (j=1,\cdots,N-1) \text{ zeros of } L_N', \tag{A3}$$
$$\omega_j = \frac{2}{N(N+1)[L_N(x_j)]^2}, \quad (j=0,\cdots,N). \tag{A4}$$

In order to carry out numerical simulations, by using the N-th order Legendre polynomials, the basis function $\varphi_i(\zeta)$ defined in one dimension is given by

$$\varphi_i(\zeta) = \frac{-1}{N(N+1)L_N(\zeta_i)}\frac{(1-\zeta^2)L_N'(\zeta)}{\zeta-\zeta_i}. \tag{A5}$$

References

1 Hirsch C. Numerical Computation of Internal and External Flows. New York: John Wiley & Sons, 1988.
2 Virieux J. P-SV wave propagation in heterogeneous media: Velocity-stress finite-difference method. Geophysics, 1986, 51: 889—901.
3 Levander A. R. Fourth-order finite-difference P-SV seismograms. Geophysics, 1988, 53: 1425—1436.
4 Wang X. M. and Zhang H. L. Modeling of elastic wave propagation on a curved free surface using an improved finite-difference algorithm. Science in China (Ser. G), 2004, 47(5): 633—648.
5 Finlayson B. A. and Scriven L. E. The method of weighted residuals-a review. Appl. Mech., 1966, (19): 735—748.
6 Hughes T. J. R. The Finite Element Method, Linear Static and Dynamic Finite Element Analysis. Englewood Cliffs, NJ: Prentice-Hall International, 1987.
7 Mu Y. G. Elastic wave migration with finite element method. Acta Geophysica Sinica, 1984, 27: 268—278.
8 Teng Y. C. Three-dimensional finite element analysis of waves in an acoustic media with inclusion. J. Acoust. Soc. Am., 1988, 86: 414—422.
9 Graves R. Simulation seismic wave propagation in 3D elastic media using staggered-grid finite differences. Bull Seism. Soc. Am., 1996, 86: 1091—1106.
10 Marfurt K. J. Accuracy of finite-difference and finite-element modeling of the scalar and elastic wave equations. Geophysics, 1984, 49: 533—549.
11 Komatitsch D. and Vilotte J. P. The spectral element method: an efficient tool to simulate the seismic response of 2D and 3D geological structures. Bull Seism. Soc. Am., 1998, 88: 368—392.
12 Orszag S. A. Spectral methods for problems in complex geometries. J. Comput. Phys., 1980, 37: 70—92.
13 Kosloff D., Kessler D., Filho A. Q. et al. Solution of the equations of dynamic elasticity by a Chebychev spectral method. Geophysics, 1990, 55: 734—748.
14 Carcione J. M. and Wang P. J. A Chebshev collocation method for the wave equation in generalized coordinates. Computers and Fluid Dynamics Journal, 1993, 2: 269—290.
15 Carcione J. M. Domain decomposition for wave propagation problems. Journal of Scientific Computing, 1991, 6(4): 453—472.
16 Patera A. T. A spectral element method for fluid dynamics: Laminar flow in a channel expansion. J. of Comput. Physics, 1984, 54: 468—488.
17 Seriani G. and Priolo E. A numerical investigation of Chebyshev spectral element method for acoustic wave propagation. In: Proc. Of 13th IMACS World Congress on Computation and Applied Mathematics. Dublin, Ireland. 1991.
18 Seriani G. A parallel spectral element method for acoustic wave modeling. J. of Compt. Acoustics, 1997, 5(1): 53—69.
19 Seriani G. Double-grid Chebshev spectral elements for acoustic wave modeling. Wave Motion, 2004, 39: 351—360.
20 Dauksher W. and Emery A. F. Accuracy in modelling the acoustic wave equation with Chebyshev spectral finite elements. Finite Elements in Analysis and Design, 1997, 26: 115—128.
21 Komatitsch D. and Tromp J. Introduction to the spectral element method for three-dimensional seismic wave propagation. Geophys J. Int., 1999, 139: 806—822.
22 Canuto C., Huaaaini M. Y., Quartteroni A. et al. Spectral Methods in Fluid Dynamics. New York: Springer-Verlag, 1986.